Chapter 4

TRIGGER AND DATA ACQUISITION

This chapter provides an introduction to the Trigger and Data Acquisition (TDAQ) system in ATLAS. The trigger system is a crucial component of the experiment, responsible for selecting events of interest at a recording rate of approximately 1 kHz from up to 40 MHz of proton-proton collisions corresponding to 25 ns bunch spacing of the LHC.

I will describe an overview and motivation triggering in section 4.1, the subsystems of the trigger system in section 4.2 during Run 2, a brief description of a trigger menu section 4.3, and discuss the data and simulated samples for the thesis analysis in section 4.4. Finally, I close off this chapter by discussing the instrumentation upgrades in section 4.2.1 for Run 3 and beyond.

4.1 Overview

During Run 1, the trigger system [2, 3, 4, 5, 6] of the ATLAS experiment operated at instantaneous luminosities of $8 \times 10^{33}\text{cm}^{-2}\,\text{s}$ with center-of-mass energies $\sqrt{s} = 7\text{–}8\,\text{TeV}$. Since 2015, the start of Run 2, the center-of-mass energy nearly doubled to 13 TeV. This increase coupled with higher luminosity and more proton-proton interactions per bunch-crossing[1] requires an efficient trigger system to maintain rates low enough to record data while maintaining the physics impact. The rest of this chapter will only describe the system from 2015 and beyond.

The TDAQ system shown in fig. 4.1 consists of a hardware-based first-level trigger (L1) and a software-based high-level trigger (HLT). The L1 trigger decision is formed by the

[1] more pileup

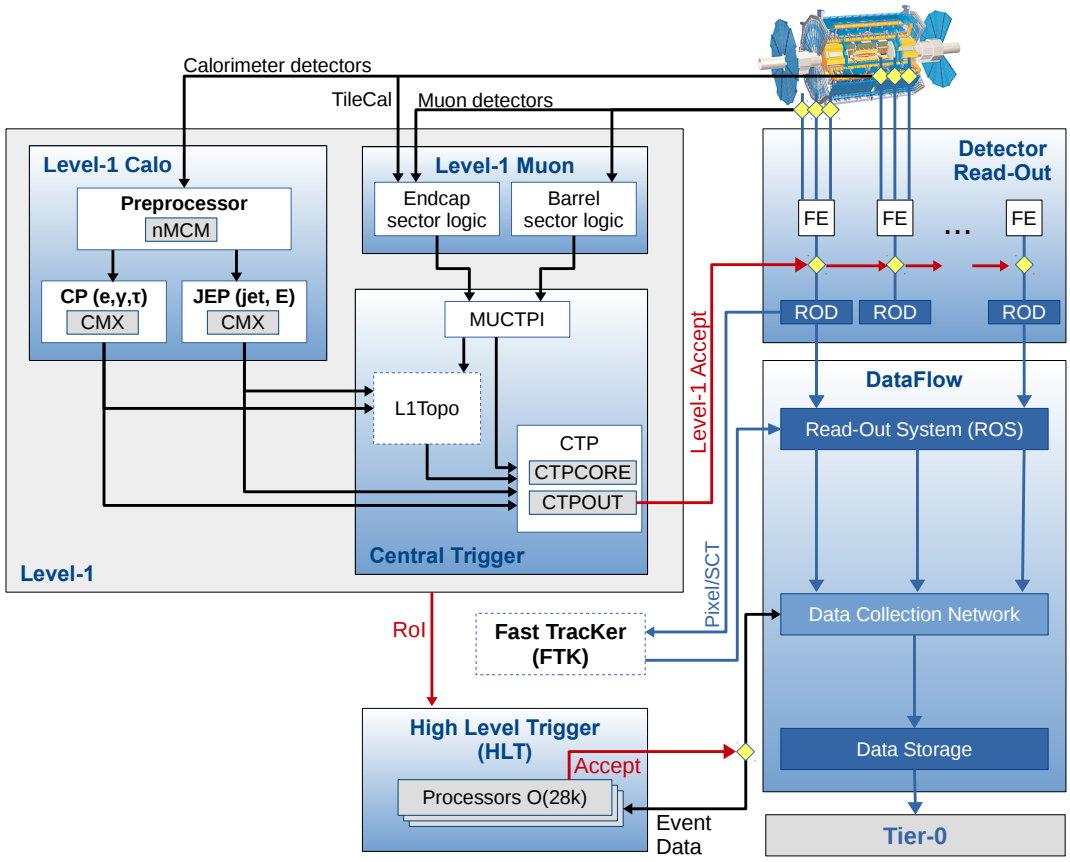

Figure 4.1: [1] A schematic overview of the ATLAS TDAQ system in Run 2 with emphasis on the components relevant for triggering. The main subsystems shown are the Level-1 (L1) trigger, the High-Level Trigger (HLT), and the Fast TracKer (FTK).

Central Trigger Processor (CTP)[2] which receives inputs primarily from L1 calorimeter trigger (L1Calo) and L1 muon trigger (L1Muon). The other role the CTP is preventative to protect front-end readout buffers from overflowing. This is known as dead-time and comes in two forms: simple and complex. Simple dead-time is the amount of time needed to allow the readout windows to process data[3]. Complex dead-time is the determined based on the rate in which the downstream front-end buffers can empty out[4]. The decision by the L1CTP is called the L1 accept (L1A) at a maximum rate of 100 kHz. Events are buffered in the readout system to be processed by the HLT which receives region-of-interests (ROIs) from the L1 subsystems for locally-based reconstruction. After the HLT acceptance at a maximum rate of 1 kHz[5], the events are transferred to local storage to be exported out to the Tier-0 computing facility[6] at European Organization for Nuclear Research (CERN) for offline reconstruction, described in more detail in **??**. Each event is 1–2 MB in size which means the readout system writes out 1–2 $\mathrm{GB\,s^{-1}}$ to disk. At the end of the day, the ATLAS detector can only save one event for every 40000 produced at the LHC. The trigger system is crucial and optimized to increase the chance of selecting the interesting, rare events for offline physics analysis.

[2]The CTP has a configurable lookup table mapping combinations of input signals to an output decision.

[3]In the start of 2015, this was set to 100 ns, or 4 bunch-crossings.

[4]This concept of rate-limiting is often otherwise called a "token bucket" or a "leaky bucket".

[5]This is a detector readout limitation.

[6]These computers are running Scientific Linux CERN (SLC), a publicly-available operating system for scientific computing.

4.2 The TDAQ Subsystems

4.2.1 Level-1 Trigger

The Level-1 Trigger is composed of two main subsystems: L1Calo and L1Muon. The L1 trigger decision, L1A, is based on the outputs of the muon spectrometer **??** and the calorimeters **??**. As the decisions need to be made quickly, all of the reconstruction algorithms are implemented in the hardware, and in some cases on FPGAs. The logic of L1Calo is much more complicated, compared to L1Muon, as it tries to identify electrons, photons, taus, jets, and calculate the missing transverse energy. As such, I expand more on the details of the L1Calo system as it will also provide the necessary context for discussing the instrumentation upgrades described in . In the rest of this section, I describe the different components that go into the L1 CTP to make a decision, accepting 1 out of every 400 events.

Level-1 Calorimeter Trigger

The L1Calo trigger receives inputs from the hadronic and electromagnetic calorimeters as described in **??**. As seen in fig. 4.1, the inputs from the calorimeter need to be preprocessed by the preprocessor system [7]. This preprocessor digitizes and calibrates the analog signals from the calorimeter detectors. In particular, a bunch-by-bunch pedestal subtraction scheme enables a significant rate reduction of the triggers used. The bunch-by-bunch correction accounts for the increased trigger rates at the beginning of a bunch train caused by the combination of in-time and out-of-time proton-proton collision events convolved with the electronic pulse signal from LAr [8, fig. 2].

The preprocessor outputs are used as inputs to the Cluster Processor (CP) and Jet/Energy Processor (JEP) subsystems in parallel. These outputs are approximately 7000 trigger tow-

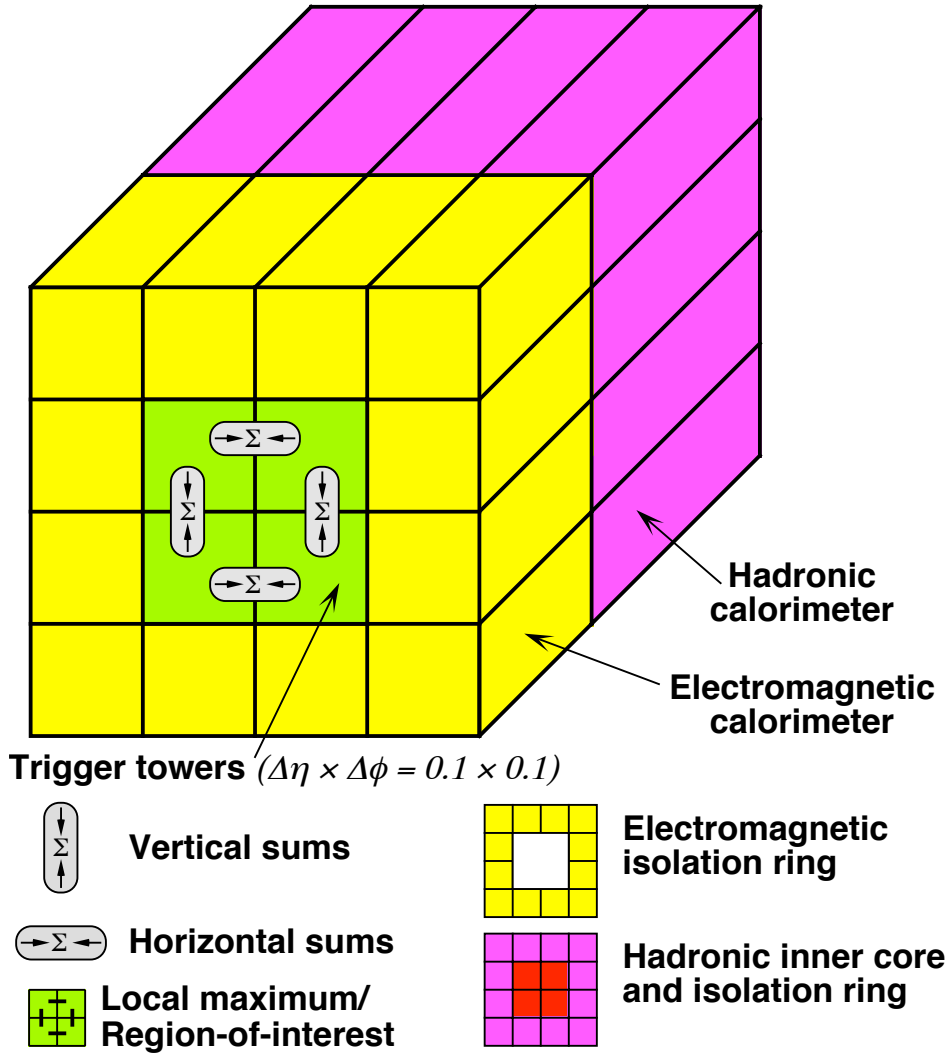

Figure 4.2: [1] A schematic view of the trigger towers used as input to the L1Calo trigger algorithms.

ers, of granularity $\Delta\eta \times \Delta\phi = 0.1 \times 0.1$, as shown in fig. 4.2. Figure 4.2 depicts the elements used for the electron/photon and tau/hadron algorithms. They are based on a sliding window of 4×4 trigger towers in both the electromagnetic and hadronic calorimeters to form six basic calculables [9][7]:

1. four 2×1 trigger tower regions are formed to measure the transverse energy of the electromagnetic showers (the vertical and horizontal sums inside the green)

2. a hadronic core (in red) of the four hadronic towers, behind the electromagnetic towers, used for isolation criteria in the hadronic calorimeters

3. four hadronic clusters which are the sum of the previous two items (1) and (2) to measure the transverse energy of hadronic showers

4. an electromagnetic isolation ring (in yellow) which consists of the twelve electromagnetic towers surrounding the core (in green), used for isolation criteria in the electromagnetic calorimeters

5. a hadronic isolation ring (in purple) which consists of the twelve hadronic towers surrounding the core (in red), used for isolation criteria in the hadronic calorimeters

6. a 2×2 ROI which is summed over both the electromagnetic and hadronic layer to identify candidate ROIs

These six calculables are used by the algorithms to identify triggerable objects. The transverse energy thresholds are configurable for different η regions[8] to account for the varying detector energy responses. There are two main modules here: Cluster Processor Module (CPM) and Jet/Energy Module (JEM).

[7]Since these firmware algorithms need to run in nanoseconds, the energy sums are scalar energy sums, rather than vector sums.

[8]Granularity here is $\Delta\eta = 0.1$

CPM To identify a 2×2 ROI as an electromagnetic trigger candidate or a hadronic trigger candidate, the electron/photon (tau/hadron) algorithm searches for narrow, highly energetic showers in the electromagnetic calorimeters: applying a threshold on the electromagnetic tower region sums, isolation criteria by applying a maximum energy threshold, and making sure the showers do not (do) penetrate into the hadronic calorimeters; respectively. If these conditions are met, the window is said to contain the respective trigger candidate.

JEM To identify a 2×2 "jet" ROI, sliding trigger tower windows of sizes 4×4 and 8×8[9] look for ROIs where the summed electromagnetic and hadronic tranverse energy exceed a predefined threshold surrounding the ROI which is a local maxima. If these criteria are met, then the window is said to contain a "jet" trigger candidate.

In the case where electronic saturation occurs, a trigger candidate is produced. These ROIs are sent to the Common Merger Extended Module (CMX) as Trigger OBjects (TOBs) which handles the logic of counting and identifying the position/energy to L1 topological processor (L1Topo). A TOB contains the transverse energy sum, η-ϕ coordinates, and isolation thresholds (where relevant), as well as identifying information to specify what kind of TOB it is[10]. Additionally, these ROIs are also sent to the HLT to seed the trigger algorithms there.

Level-1 Muon Trigger

In parallel to L1Calo in section 4.2.1, the L1Muon system looks for coincidences in different layers of the muon chambers. Extra logic exists to reject muons that do not originate from

[9] A 4×4 (8×8) window size is 0.4×0.4 (0.8×0.8) in $\Delta\eta \times \Delta\phi$.

[10] Identifying information such as a `JET` TOB or a `EM` TOB, etc.

the primary vertex. Events with muons with large transverse energy compared against a predefined threshold are selected and sent to L1Topo, through the Muon-to-CTP interface (MUCTPI), for a decision.

4.2.2 HLT

After the L1A, the events are processed by the HLT using finer-granularity calorimeter information, measurements from the muon spectrometer (MS), and tracking information[11] from the ID. The HLT runs on a processing farm to perform a subset of offline event reconstruction. The lower input rate and software-based reconstruction allows for more complex and configurable trigger decisions. There are, however, some computational limitations such as track reconstruction that necessitates an upgrade, FTK, being commissioned[12] in 2017 to allow for full tracking information at the HLT. The FTK is briefly described in section 4.2.2

FTK

A new FTK system [10] will provide global ID track reconstruction at the L1 trigger rate using lookup tables stored in custom associative memory chips for the pattern matching capabilities for every event that contains a L1A. The FPGA-based track fitter performs a fast linear fit and the tracks are made available to HLT, allowing the use of tracks at a rate much higher than capable with a CPU-based system. Since the FTK provides a hardware-based tracking solution that can handle the challenge of high luminosity, it allows ATLAS to maintain trigger thresholds such as the ability to reconstruct and identify secondary

[11] Note that the tracking information from the Inner Detector (ID) is not available at L1

[12] This is a rather generic term that refers to both the process of making the reconstruction algorithms work as intended (commissioning of reconstructed objects) and the process of understanding how what is reconstructed in the detector corresponds to what actually happened in the detector (detector commissioning).

vertices[13].

4.3 Trigger Menu

The trigger menu [1] defines a list of L1 and HLT triggers and consists of five different flavors of triggers:

1. primary triggers – used for physics analyses and are typically unprescaled[14]
2. support triggers – used for efficiency measurements, performance measurements, and monitoring
3. alternative triggers – used for experimental/new triggers that overlap significantly with primary triggers – but could be useful for a specific analysis or purpose
4. backup triggers – like primary triggers but with tighter selections and a lower expected rate
5. calibration triggers – used for calibration effort

When the LHC beams are colliding, multiple trigger menus are defined and available to be used. The rate and bandwidth constraints of the ATLAS detector, TDAQ, and offline computing are dependent on the luminosity and average number of proton-proton collisions. Therefore, the menu[15] is defined for a given range of luminosity that provides an expected output rate during detector operation. The two most relevant constaints are 100 kHz for L1 and 1 kHz for HLT, the former is limited by ATLAS readout capability and the latter is

[13]This is important in analyses that are sensitive to b-tagging for example, but this is explained more in **??**.

[14]If a trigger is prescaled, this means the trigger rate is purposefully decreased in order to keep the output rate manageable.

[15]It can, and is, also defined for different types of bunch grouping from the LHC.

limited by offline computing power. Trigger names all have the same pattern, as also used throughout this thesis later on, which consist of:

1. Trigger level: `L1` or `HLT`
2. Multiplicity: `SINGLE`, `MULTI`, $n \in \mathbb{Z}$
3. Object type: `el` for electron, `mu` for muon, `j` for jet, `xe` for missing transverse energy, `te` for transverse energy
4. Threshold value in GeV
5. Seeded L1 trigger (if describing an HLT trigger)

So for example:

- `HLT_MU20_L1MU15` describes an HLT trigger requiring a 20 GeV muon candidate which is seeded by an L1 trigger requiring a 15 GeV muon candidate
- `HLT_xe70` describes an HLT trigger requiring 20 GeV of missing transverse energy

4.4 Data and simulated event samples

The data used in this analysis were collected by the ATLAS detector from pp collisions produced by the LHC at a centre-of-mass-energy of 13 TeV and 25 ns proton bunch spacing over the 2015 and 2016 data-taking periods. The full dataset corresponds to an integrated luminosity of 36.1 fb^{-1} after the application of beam, detector and data-quality requirements. The uncertainty in the combined 2015+2016 integrated luminosity is 2.1%. It is derived, following a methodology similar to that detailed in [11], from a preliminary calibration of the

luminosity scale using x–y beam-separation scans performed in August 2015 and May 2016. Events are required to pass a $E_{\mathrm{T}}^{\mathrm{miss}}$ trigger with thresholds of 70 GeV, 100 GeV and 110 GeV at the HLT level for the 2015, early 2016 and late 2016 datasets, respectively. These triggers are fully efficient for events passing the preselection defined in **??**, which requires the offline reconstructed $E_{\mathrm{T}}^{\mathrm{miss}}$ to exceed 200 GeV. There are on average 24 inelastic pp collisions (see **??**) in the dataset.

Samples of monte-carlo (MC) simulated events are used to model the signal and background processes in this analysis, except multijet processes, which are estimated from data. Supersymmetry (SUSY) signal samples in which each gluino decays as $\tilde{g} \to t\bar{t}\tilde{\chi}_1^0$ were generated with up to two additional partons using MadGraph5_aMC@NLO [12] v2.2.2 at leading order (LO) with the NNPDF 2.3 [13] parton distribution function (PDF) set. These samples were interfaced to Pythia v8.186 [14] for the modeling of the parton showering, hadronization and underlying event.

The dominant background in the signal regions is the production of $t\bar{t}$ pairs with additional high p_{T} jets. For the generation of $t\bar{t}$ and single top quarks in the Wt-channel and s-channel the Powheg-Box [15] v2 event generator with the CT10 [16] PDF set in the matrix element calculations was used. Electroweak t-channel single-top-quark events were generated using the Powheg-Box v1 event generator. This event generator uses the four-flavour scheme for the next-to-leading-order (NLO) matrix elements calculations together with the fixed four-flavour PDF set CT10f4. For all processes involving top quarks, top-quark spin correlations are preserved. In the t-channel, top quarks were decayed using MadSpin [17]. The parton shower, fragmentation, and the underlying event were simulated using Pythia v6.428 [18] with the CTEQ6L1 PDF set [19]. The h_{damp}[16] parameter in Powheg, which controls the p_{T} of the first additional emission beyond the Born level and thus regulates the p_{T} of the

[16]This is a parameter that will be varied for theory systematics, as described in **??**.

recoil emission against the $t\bar{t}$ system, was set to the mass of the top quark ($m_{\text{top}} = 172.5$ GeV). All events with at least one leptonically decaying W boson are included. Single-top and $t\bar{t}$ events in which all top quarks decay hadronically do not contain sufficient $E_{\text{T}}^{\text{miss}}$ to contribute significantly to the background.

Smaller backgrounds in the signal region come from the production of $t\bar{t}$ pairs in association with $W/Z/h$ bosons and possibly additional jets, and production of $t\bar{t}t\bar{t}$, W/Z+jets and $WW/WZ/ZZ$ (diboson) events. Other potential sources of background, such as the production of three top quarks or three gauge bosons, are expected to be negligible. The production of $t\bar{t}$ pairs in association with electroweak vector bosons W and Z was modeled by samples generated at LO using MadGraph5_aMC@NLO v2.2.2 and showered with Pythia v8.186, while samples to model $t\bar{t}H$ production were generated using MadGraph5_aMC@NLO v2.2.1 and showered with Herwig++ [20] v2.7.1. These samples are described in detail in [21]. MadGraph5_aMC@NLO was also used to simulate the $t\bar{t}t\bar{t}$ production and the showering was performed with Pythia v8.186. The W/Z+jets processes were simulated using the Sherpa v2.2.0 [22] event generator, while Sherpa v2.1.1 was used to simulate diboson production processes. Matrix elements for the W/Z+jets and diboson processes were calculated using Comix [23] and OpenLoops [24] and merged with the Sherpa parton shower [25] using the ME+PS@NLO prescription [26]. The Sherpa diboson sample cross-section was scaled down to account for its use of $\alpha_{\text{QED}} = 1/129$ rather than $\alpha_{\text{QED}} = 1/132$, corresponding to the use of current Particle Data Group [27] parameters, as input to the G_μ scheme [28]. Samples generated using MadGraph5_aMC@NLO v2.2.2 were produced with the NNPDF 2.3 PDF set and W/Z+jets samples were generated with the NNPDF 3.0 PDF set [29], while all other samples used CT10 PDFs.

All simulated event samples were passed through the full ATLAS detector simulation using Geant4 [30]. The simulated events are reconstructed with the same algorithm as that used

for data. For all samples, except the ones generated using SHERPA, the EVTGEN v1.2.0 program [31] was used to simulate the properties of the bottom- and charm-hadron decays. All PYTHIA v6.428 samples used the PERUGIA2012 [32] set of tuned parameters (tune) for the underlying event, while PYTHIA v8.186 and HERWIG++ showering were run with the A14 [33] and UEEE5 [34] underlying-event tunes, respectively. In-time and out-of-time pile-up interactions from the same or nearby bunch-crossings were simulated by overlaying additional pp collisions generated by PYTHIA v8.186 using the A2 tune [35] and the MSTW2008LO parton distribution function set [36] on top of the hard-scattering events. Details of the sample generation and normalization are summarized in table 4.1. Additional samples with different event generators and settings are used to estimate systematic uncertainties in the backgrounds, as described in **??**.

The signal samples are normalized using the best cross-section calculations at NLO in the strong coupling constant, adding the resummation of soft gluon emission at next-to-leading-logarithm (NLL) accuracy [37, 38, 39, 40, 41]. The nominal cross-section and the uncertainty are taken from an envelope of cross-section predictions using different PDF sets and factorization and renormalization scales, as described in [42]. The cross-section of gluino pair-production in these simplified models is $14 \pm 3\,\text{fb}^{-1}$ for a gluino mass of 1.5 TeV, falling to $1.0 \pm 0.3\,\text{fb}^{-1}$ for 2 TeV mass gluino. This is also summarized in table 4.1.

Finally, contributions from multijet background are estimated from data using a procedure described in [43], which performs a smearing of the jet response in data events with well-measured $E_{\text{T}}^{\text{miss}}$ (so-called "seed events"). The response function is derived in Monte Carlo dijet events and is different for b-tagged and non-b-tagged jets.

The specific list of samples used in the analysis are shown in **??**.

Process	Event Generator + fragmentation/hadronization	Tune	PDF set	Cross-section order
SUSY signal	MadGraph5_aMC@NLO v2.2.2 + Pythia v8.186	A14	NNPDF2.3	NLO+NLL [37, 38, 39, 40, 41, 42]
$t\bar{t}$	Powheg-Box v2 + Pythia v6.428	PERUGIA2012	CT10	NNLO+NNLL [44]
Single top	Powheg-Box v1 or v2 + Pythia v6.428	PERUGIA2012	CT10	NNLO+NNLL [45, 46, 47]
$t\bar{t}W/t\bar{t}Z$**/4-tops**	MadGraph5_aMC@NLO v2.2.2 + Pythia v8.186	A14	NNPDF2.3	NLO [48]
$t\bar{t}H$	MadGraph5_aMC@NLO v2.2.1 + Herwig++ v2.7.1	UEEE5	CT10	NLO [49]
Diboson WW, WZ, ZZ	Sherpa v2.1.1	Default	CT10	NLO [28]
W/Z**+jets**	Sherpa v2.2.0	Default	NNPDF3.0	NNLO [50]

Table 4.1: List of event generators used for the different processes. Information is given about the underlying-event tunes, the PDF sets and the pQCD highest-order accuracy used for the normalization of the different samples.

4.5 ATLAS Trigger System Phase-I Upgrade

The current L1Calo trigger system functions with relatively high-resolution identification of events with a wide-variety of objects including electron, photons, tau-leptons, and jet objects, along with missing transverse energy. A detailed description of LAr Calorimeter Phase-I Upgrade design can be found in [51, 52] following the schedule of the LHC upgrade described in **??**. In order to maintain a high trigger acceptance and trigger rate for these objects, LAr plans to provide finer granularity by means of super-cells which are up to $\Delta\eta \times \Delta\phi = 0.025 \times 0.1$ providing information for each calorimeter layer. The planned L1Calo Feature EXtractors (FEXs) will take advantage of this increased granularity.

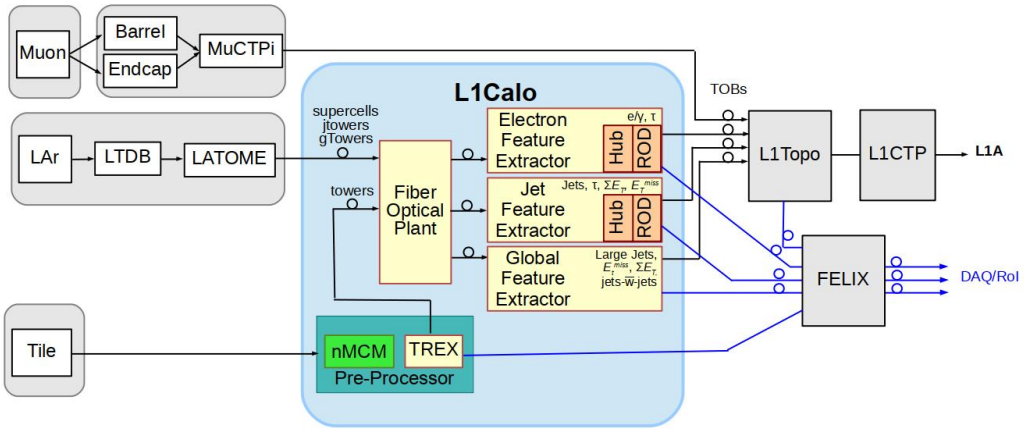

Figure 4.3: [53] The L1Calo system following the completion of the Phase-I upgrade at the start of Run 3. The new elements include the L1Calo PreProcessor Module (PPM), Optical Plant, Hub, ReadOut Driver (ROD), and the three FEXs: electron Feature EXtractor (eFEX), jet Feature EXtractor (jFEX), and gFEX.

Figure 4.3 shows the The LAr Trigger Digitizer Boards (LTDBs) will digitize and transmit the input calorimeter signals to LATOME cards. The FPGA on each LATOME card will reconstruct the transverse energy of each super-cell and then transmits this information

to each of the FEXs. Both jFEX and eFEX are meant to provide similar, yet improved functionality for the CPMs and JEMs while gFEX [53] is a completely new addition that will be added as part of the Phase-I upgrade. After a L1A, the LAr Digital Processing System (LDPS) and FEXs deliver output data to the TDAQ readout chain via Front-End Link EXchange (FELIX) [54], a multi-purpose routing device that interfaces the various ATLAS sub-detectors to the data acquisition system. In order to allow for appropriate commisioning of these new FEXs, the LTDB will also send the legacy trigger towers ($\Delta\eta \times \Delta\phi = 0.1 \times 0.1$) to the current L1Calo preprocessor and along the path described in section 4.2.1.

In the following subsection, I describe how gFEX plans to fit in the system and Chicago's unique role in this forward-facing project for Phase-I.

4.5.1 The Global Feature Extractor Module

The gFEX concept was introduced in mid-2013 and I joined the team shortly. This is an on-going project and the physics motivations are presented in **??**. A block diagram of the gFEX module is shown in fig. 4.4 with a constructed board in fig. 4.5. A special feature of this subsystem is that it receives data from the entire calorimeter with a single electronics module. This maximizes trigger capability and flexibility for future trigger menus. The requirement of a single module imposes unique constraints on the design of this board. In order to be installed by the ATLAS detector and allow for reasonable temperature/power usage, up to four FPGAs can reasonably fit on the board.

There are three large Processor FPGAs (pFPGAs) for data processing and a Zynq+® from Xilinx that combines an FPGA and a CPU into a System-on-Chip (SoC). Chicago's role is to provide slow-control and monitoring of gFEX through the Zynq+®. The design is

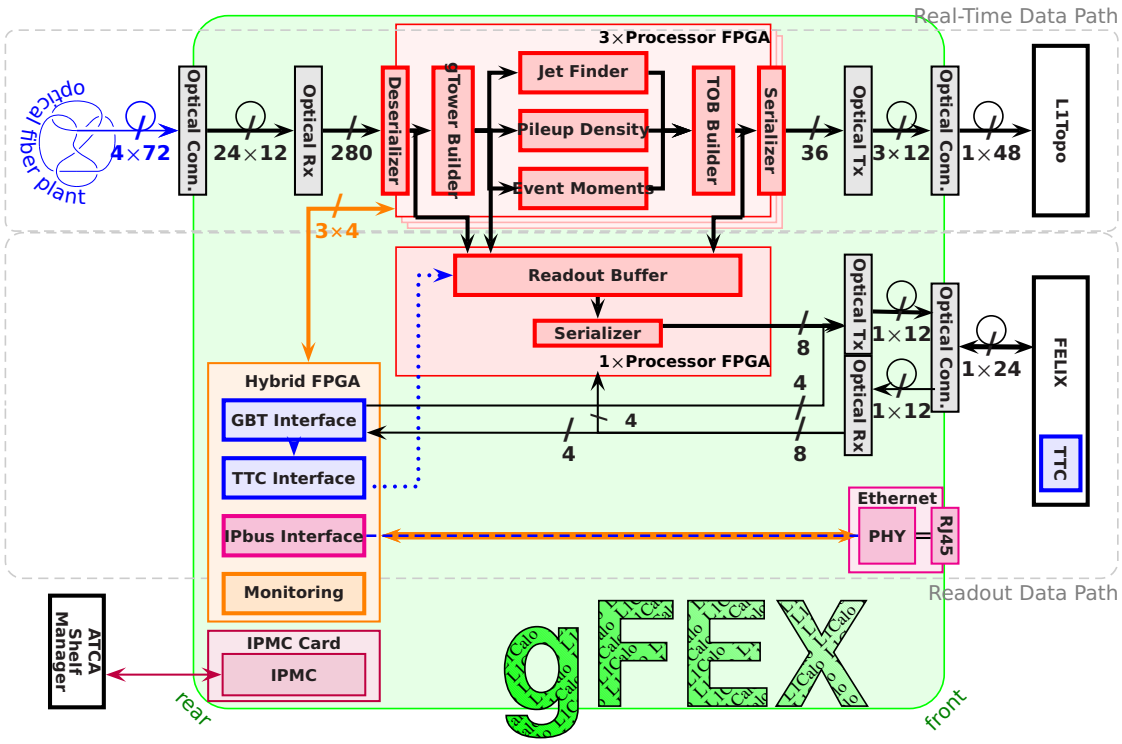

Figure 4.4: [53] A block diagram of the gFEX module. Shown are the real-time (to L1Topo) and readout (to FELIX) data paths. The Zynq+® is also shown.

for each of the three pFPGAs to have 100 high-speed links[17] for input calorimeter data and output TOBs, ROIs, and calorimeter data. Unlike the design of other FEXs, gFEX allocates more fibers to carrying calorimeter output than for intra-FPGA communications. Each pFPGA has 2π azimuthal coverage for a given slice in η and executes all feature identification algorithms. Two pFPGAs handle the central $|\eta| < 2.5$ region receiving data from electromagnetic calorimeter (EMCal) and hadronic calorimeter (HCal) with the third pFPGA handling the forward $2.5 < |\eta| < 4.9$ region receiving data from EMCal, HCal, and forward calorimeter (FCal).

The FPGA on the Zynq+®, known as the Zynq FPGA (zFPGA), is also employed in the calculation of global quantities. Towers from LATOME containing calorimeter data are $\Delta\eta \times \Delta\phi = 0.2 \times 0.2$, known as gCaloTowers, are summed across layers to form gTowers

[17] Also known as fibers.

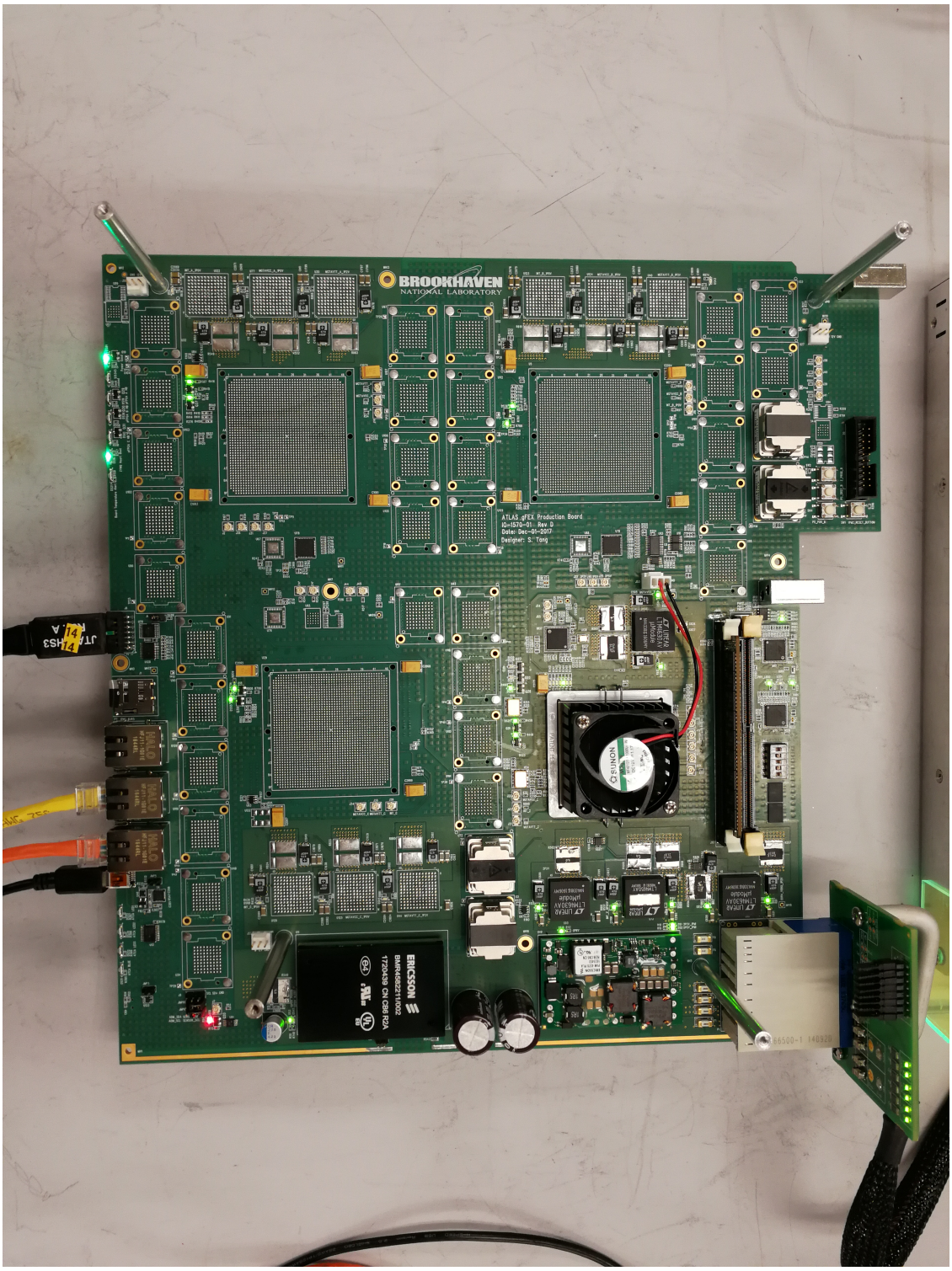

Figure 4.5: A picture of the gFEX v4 board at Brookhaven National Lab. The three pFPGAs have not been placed yet. The Zynq+® is placed with a heat-sink and fan on top in the lower-right. This board has successfully loaded the custom Linux kernel I built along with the "iroman" slow-control and monitoring software.

which are used as inputs to algorithms on the pFPGAs that need to run in 5 Bunch Crossings (BCs) latency.

Latency (BC)	pFPGA	zFPGA
2.0	receiver & deserialization	
1.0	demultiplexing & synchronization	
5.0	primitive processing (Algorithms)	
1.0	TOB selection for output	global fragment transfers
1.0	TOB selection for output	global TOB processing
1.0	multiplexing	multiplexing
2.0	transmitter & serialization	transmitter & serialization
2.0	optical fiber to L1Topo (10 m)	optical fiber to L1Topo (10 m)
15.0	Total latency for gFEX	

Table 4.2: [53] Latency profile of the real-time trigger path for the gFEX. The maximum latency envelope is 15 BCs including transmission to the L1Topo.

Physics objects and observables are reconstructed by very fast fixed-latency algorithms in firmware running on the pFPGAs and zFPGA. These identified features are used in the L1 trigger decision. These algorithms have 5 BCs to run, out of a tentative total latency of 15 BCs given to gFEX for Run 3, as described in table 4.2. These algorithms currently include tower building to form gTowers[18], pile-up suppression, and calculations for: jet multiplicity, jet substructure, total and missing transverse energy. An illustration of gTower segmentation and gBlock formation is shown in fig. 4.6.

More algorithms are being designed and tested through the entire gFEX development and commissioning process. More details on some of the physics studies being performed are shown in **??**. After these algorithms finish processing, the zFPGA steps in the role of

[18]While gTowers are useful from a physics perspective, latency requirements forces us to be a little bit clever about the design of the algorithms on firmware. A contiguous group of gTowers are formed into gBlocks, as long as the scalar sum of gTower energy is greater than a threshold, which are used as common inputs to the algorithm firmware.

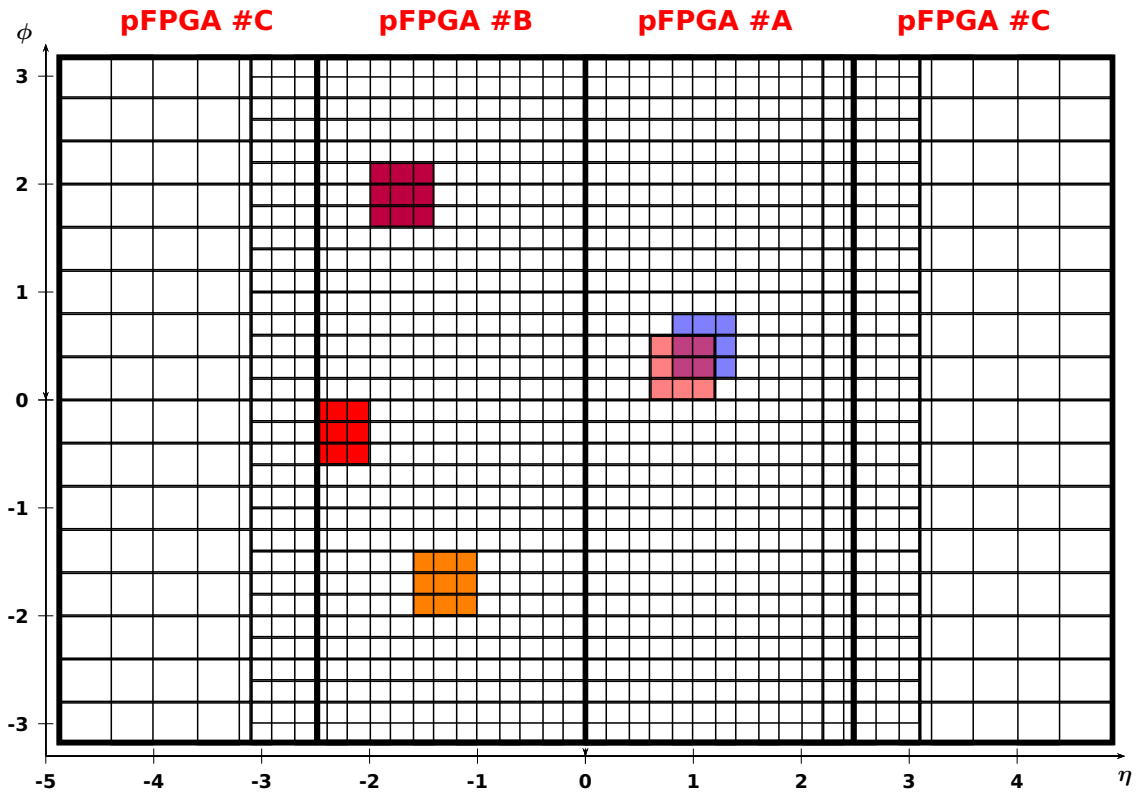

Figure 4.6: [53] gTower segmentation in the calorimeter. Note the special gTower coverage at $2.4 < |\eta| < 2.5$ and $3.1 < |\eta| < 3.2$. The central regions covered by pFPGA 1 and pFPGA 2 contain primarily gTowers of size up to $\Delta\eta \times \Delta\phi = 0.2 \times 0.2$ and the forward regions have up to $\Delta\eta \times \Delta\phi = 0.4 \times 0.4$. gBlock formation is also illustrated in colors here as contiguous blocks of gTowers, often 3×3. Note that gBlocks in an event are allowed to overlap. Also note that not all gBlocks have the same size.

forming TOBs which contain global quantities, such as pileup and missing transverse energy, and quantities related to jet candidates, such as jet multiplicity, found with the algorithms. These TOBs are sent to L1Topo for a decision. A trigger menu will be designed based on the rates of certain objects. For example, fig. 4.7 shows a study of rates that I did for gFEX where there was an average of 80 and 200 proton-proton collisions per event, high luminosity and high pileup.

For example, in order to obtain a 10 kHz rate with a single gTower trigger, a 80 GeV threshold needs to be set for events with an average of 80 proton-proton collisions, while a 95 GeV threshold needs to be set for events with an average of 200 proton-proton collisions.

If one were to design a trigger menu based on these results from gFEX for $\langle\mu\rangle = 200$, `L1_GFEX_1T95`, `L1_GFEX_2T55`, and `L1_GFEX_4B35` are possible items providing a 10 kHz rate. This study is preliminary and further work needs to be done to understand the rates of the TOBs provided by gFEX for commissioning and trigger menu definition. Some studies on the efficiency of the trigger are provided in **??**.

4.5.2 Slow Control and Monitoring of gFEX

In order to ensure that the gFEX module functions properly through the entirety of an experiment, it is important to be able to flag problematic data and to detect when the board is under excessive load before it affects other subsystems and the experiment as a whole. The gFEX has a complete snapshot of the calorimeter information for each event and a Zynq+® capable of processing this data. Calorimeter information can be sent[19] to the Zynq+® for further processing based upon:

- an error flag from the calorimeter data (such as a failed checksum)

[19] At a rate less than the bunch crossing rate of 40 MHz.

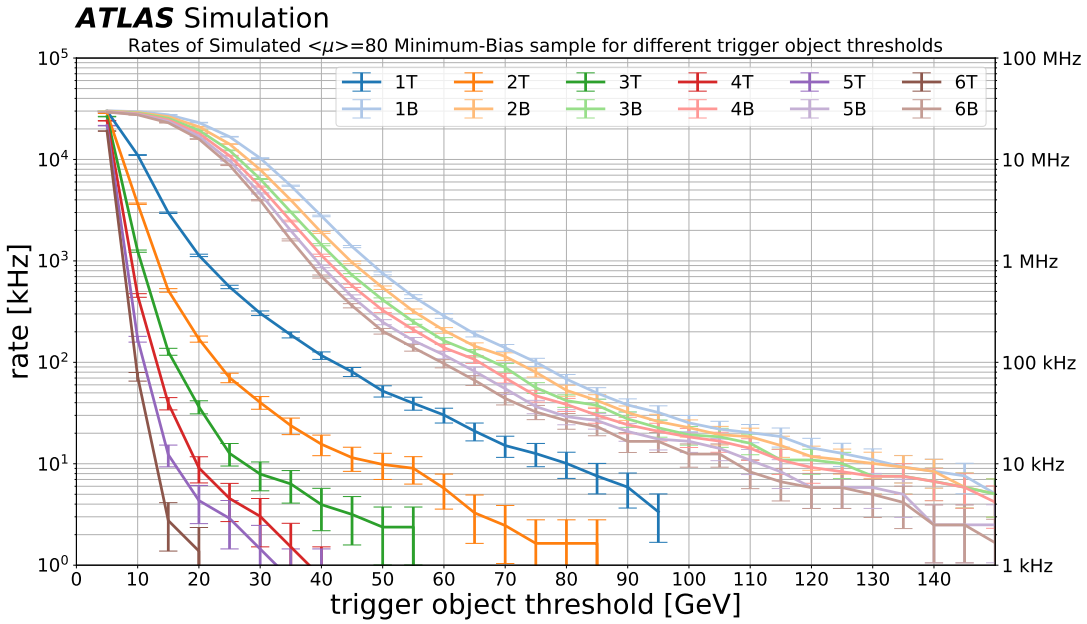

(a) $\langle\mu\rangle = 80$

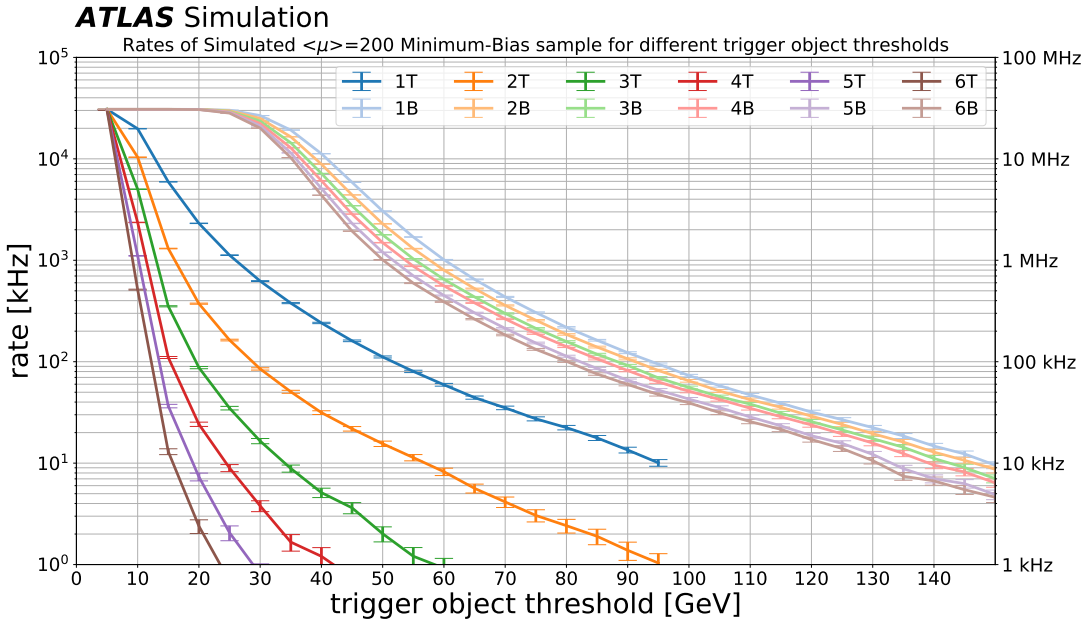

(b) $\langle\mu\rangle = 200$

Figure 4.7: gFEX rates shown for a simulated sample with (a) 80 and (b) 200 proton-proton interactions, representing potential data events for High Luminosity LHC (HL-LHC). Each curve corresponds to a different trigger item requiring one, two, or more gFEX trigger objects (gTowers [dark curves], gBlocks [light curves]) with the x-axis representing the energy threshold required for the trigger object and the y-axis showing the potential rate for the given selection. A lower threshold can provide a highly efficient trigger while maintaining rates based on the readout capabilities of the ATLAS detector.

- a signal or flag from the FEX algorithms
- a period clock
- an external signal

This last bullet point is of note as this external signal is a command sent from the ATLAS control room over a networking interface. The monitoring framework will be capable of sampling the data to provide reports of the health of gFEX at various levels. For example, the health of the board can be reported through histograms of calorimeter channels with errors; errors in an event can be detected by emulating the FEX algorithms on the CPU of the Zynq+®; or time-dependent errors such as flagging errors correlated amongst many BCs.

Having a SoC provides many benefits by allowing an operating system to be loaded directly on gFEX and programmed using modern programming languages, such as Python, to provide a maintainable and flexible interface. Unlike the firmware written for FPGA which requires updates and changes when using a different chip, software remains largely the same as the kernel loads and unloads the necessary drivers to interface with the different hardware. It is important to gFEX to switch hardware as the full module and final design is realized as a series of incrementally improved boards for testing different components. Since joining gFEX, I have developed "meta-l1calo" – a full suite of tools for compiling a Linux kernel from scratch incorporated with specific tools such as Python and I2C (I^2C) drivers; and ironman – an open-sourced, single-threaded monitoring framework written in Python to be used on SoCs in L1Calo to connect control and monitoring requests with hardware in a transport-neutral way. The technical details of "meta-l1calo" and ironman are described in **????**. Because of this flexibility, you can customize the gFEX to present itself as a representational state transfer application programming interface (RESTful API), borrowing from modern techniques used to power the internet today, such as querying for monitoring data to be

populated by navigating with your browser as demonstrated in fig. 4.8. This software has been successfully deployed on multiple iterations of gFEX boards and can reduce the learning curve for slow-control and monitoring on custom SoCs.

As ironman is single-threaded, one can take advantage of of Multi-Processor SoCs (MPSoCs) like Zynq+® to run different, multiple instances of ironman can run in parallel with different functionalities. An instance of ironman can run slow-control for the I^2C and clock configuration, separately from an instance running monitoring of the on-board temperature and power usage. This separation of concerns and modularity allows the board to function for the next 20 years with minimal expert intervention.

4.5.3 Trigger-Aware Analysis Software

An integral part of introducing instrumentation to the ATLAS detector is having the ability to monitor the gFEX performance in order to spot trouble before it affects the experiment as a whole. The gFEX can also be used to monitor actual physics, for example, we can keep track of when the missing transverse energy is higher than normal for several sequential bunch crossings. Monitoring is controlled by the Zynq+® which receives and process the calorimeter data and interacts with the other components of the L1Calo system. The Zynq+® will also interact with non-L1Calo systems like external servers for logging.

Trigger-aware analysis has not yet been implemented. The readout size for every gTower is approximately 16.4 kB/event (15 bit × 1120 gTowers). Only reading out the TOBs would be less than 1.75 kB/event. This information could be read out directly to a dedicated stream for analysis of the gFEX TOBs offline.

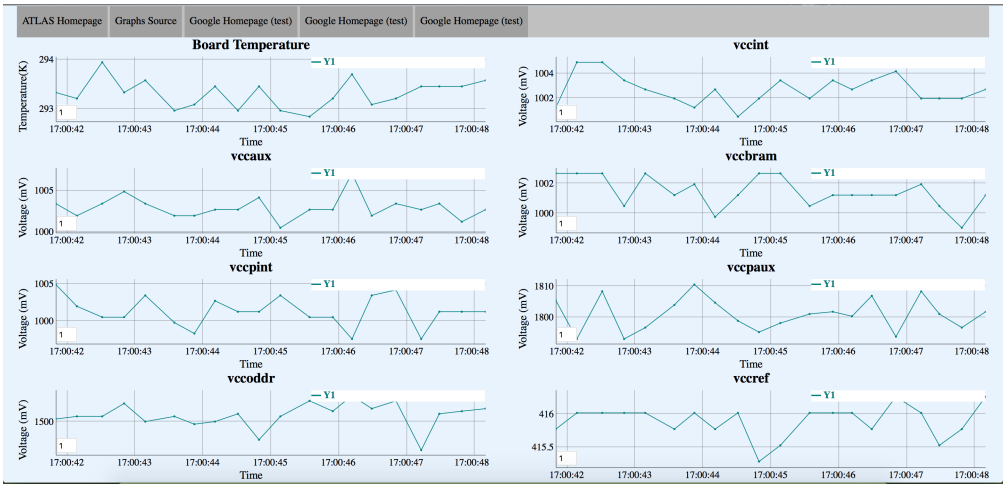

(a) Website + Javascript

```
root@gfex-prototype4:~# ./gfex_minipods.py
------------MiniPODs connected to ZYNQ Ultrascale+------------------
Refdes    Type    Temperature(C)    3.3V Power(V)    2.5V Power(V)  LOS[11:0]
U3        TX      38                3.263            2.432                111111111111
U24       TX      33                3.296            2.427
U56       TX      35                3.276            2.448
U72       RX      34                3.328            2.456
```

(b) Command Line + Python

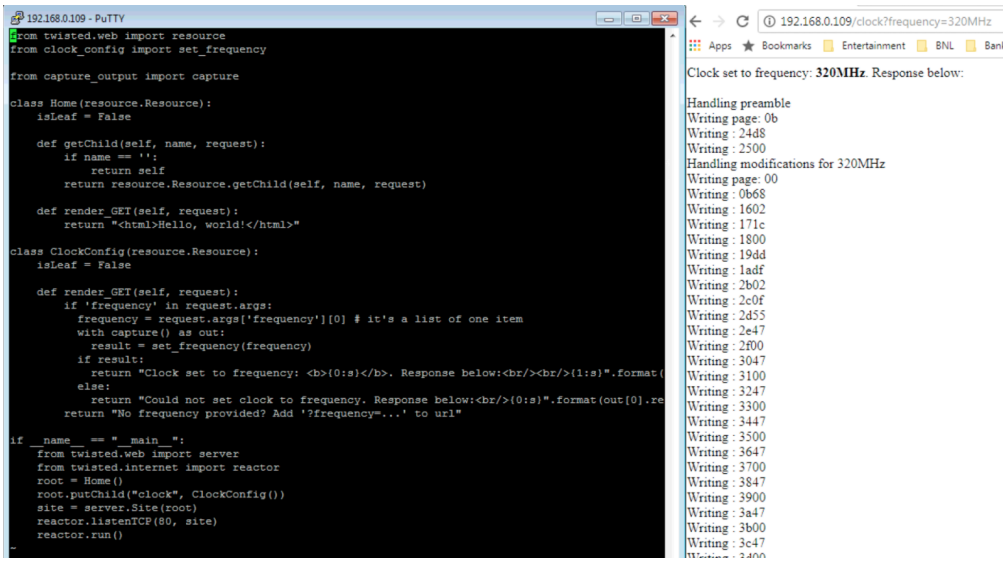

(c) Website + RESTful

Figure 4.8: Demonstration of `ironman`'s flexibility and adaptability to various programming languages and data transfer models. The flexibility is demonstrated by (a) a website with Javascript polling the board, (b) direct access over SSH with Python, and (c) a RESTful server running on the board.

Glossary

ATLAS a general-purpose detector at the Large Hadron Collider (LHC). 24, 25

BC Bunch Crossing. 20, 24

bunch train a group of bunches. 4

CERN European Organization for Nuclear Research. 3

CMX Common Merger Extended Module. 7

CP Cluster Processor. 4

CPM Cluster Processor Module. 6, 7, 17

CTP Central Trigger Processor. 1, 3, 4, 8

eFEX electron Feature EXtractor. 16, 17

EMCal electromagnetic calorimeter. 18

FCal forward calorimeter. 18

FELIX Front-End Link EXchange. 17, 18

FEX L1Calo Feature EXtractor. 16–18, 24

FPGA Field Programmable Array. 4, 8, 16–18, 24

FTK Fast TracKer. 2, 8

gBlock Group of contiguous gTowers. Most have a size of 0.6×0.6 in $\Delta\phi \times \Delta\eta$.. 20, 21, 23

gCaloTower Calorimeter tower transmitted to the gFEX. Most have a size of 0.2×0.2 in $\Delta\phi \times \Delta\eta$.. 20

gFEX global Feature EXtractor.

gTower Tower, formed by summing electromagnetic & hadronic gCaloTowers, as used on the gFEX . Most have a size of 0.2×0.2 in $\Delta\phi \times \Delta\eta$.. 20–23, 25

HCal hadronic calorimeter. 18

HL-LHC High Luminosity LHC. 23

HLT High-Level Trigger. 1–3, 7–10

Hub Common readout infrastructure for L1Calo. The ROD is a daughter card.. 16

I^2C I2C. 24, 25

ID Inner Detector. 8

ironman Transport-neutral, single-threaded Python framework to connect external users to board-specific hardware.. 24, 25

JEM Jet/Energy Module. 6, 7, 17

JEP Jet/Energy Processor. 4

jFEX jet Feature EXtractor. 16, 17

L1 Level-1. 1–4, 7–10, 20

L1A L1 accept. 3, 4, 8, 17

L1Calo L1 calorimeter trigger. 3–5, 7, 16, 17, 24

L1Muon L1 muon trigger. 3, 4, 7

L1Topo L1 topological processor. 7, 8, 18, 20, 22

LAr Liquid Argon Calorimeter. 4, 16

LATOME LAr Trigger prOcessing MEzzanine. Mezzanine card for LAr Carrier Board. Together these form the LDPB.. 16, 18

LDPS LAr Digital Processing System. 17

LO leading order. 11

LTDB LAr Trigger Digitizer Board. 16, 17

MC monte-carlo. 11

monte-carlo simulated event using random numbers. 11

MPSoC Multi-Processor SoC. 25

MS muon spectrometer. 8

MUCTPI Muon-to-CTP interface. 8

NLL next-to-leading-logarithm. 13

NLO next-to-leading-order. 11, 13

PDF parton distribution function. 11, 12

pFPGA Processor FPGA. 17–21

PPM L1Calo PreProcessor Module. 16

ROD ReadOut Driver. 16

ROI region-of-interest. 3, 6, 7, 18

SoC System-on-Chip. 17, 24, 25

super-cell LAr calorimeter region formed by summing transverse energy from cells that are adjacent in η and ϕ.. 16, 17

SUSY Supersymmetry. 11

TDAQ Trigger and Data Acquisition. 1, 2, 9, 17

TOB Trigger OBject. 7, 18, 20, 22, 25

zFPGA Zynq FPGA. 18, 20, 22

Zynq+® A Xilinx MPSoC composed of an FPGA, ARM processor, real-time processor, and a MALI-400 GPU.. 17–19, 22, 24, 25

Bibliography

[1] ATLAS Collaboration. "Performance of the ATLAS Trigger System in 2015". In: *Eur. Phys. J. C* 77 (2017), p. 317. DOI: 10.1140/epjc/s10052-017-4852-3. arXiv: 1611.09661 [hep-ex] (cit. on pp. 2, 5, 9).

[2] ATLAS Collaboration. "Performance of the ATLAS Trigger System in 2010". In: *Eur. Phys. J. C* 72 (2012), p. 1849. DOI: 10.1140/epjc/s10052-011-1849-1. arXiv: 1110.1530 [hep-ex] (cit. on p. 1).

[3] ATLAS Collaboration. *Performance of the ATLAS Electron and Photon Trigger in pp Collisions at $\sqrt{s} = 7$ TeV in 2011*. ATLAS-CONF-2012-048. 2012. URL: https://cds.cern.ch/record/1450089 (cit. on p. 1).

[4] ATLAS Collaboration. "Performance of the ATLAS muon trigger in *pp* collisions at $\sqrt{s} = 8$ TeV". In: *Eur. Phys. J. C* 75 (2015), p. 120. DOI: 10.1140/epjc/s10052-015-3325-9. arXiv: 1408.3179 [hep-ex] (cit. on p. 1).

[5] ATLAS Collaboration. "Identification and energy calibration of hadronically decaying tau leptons with the ATLAS experiment in *pp* collisions at $\sqrt{s} = 8$ TeV". In: *Eur. Phys. J. C* 75 (2015), p. 303. DOI: 10.1140/epjc/s10052-015-3500-z. arXiv: 1412.7086 [hep-ex] (cit. on p. 1).

[6] ATLAS Collaboration. "The performance of the jet trigger for the ATLAS detector during 2011 data taking". In: *Eur. Phys. J. C* 76 (2016), p. 526. DOI: 10.1140/epjc/s10052-016-4325-0. arXiv: 1606.07759 [hep-ex] (cit. on p. 1).

[7] ATLAS Level-1 Calorimeter Trigger collaboration. "The ATLAS Level-1 Calorimeter Trigger: PreProcessor implementation and performance". In: *Journal of Instrumentation* 7.12 (2012), P12008. URL: http://stacks.iop.org/1748-0221/7/i=12/a=P12008 (cit. on p. 4).

[8] ATLAS Collaboration. "Drift Time Measurement in the ATLAS Liquid Argon Electromagnetic Calorimeter using Cosmic Muons". In: *Eur. Phys. J. C* 70 (2010), p. 755. DOI: 10.1140/epjc/s10052-010-1403-6. arXiv: 1002.4189 [hep-ex] (cit. on p. 4).

[9] E F Eisenhandler. *ATLAS Level-1 Calorimeter Trigger Algorithms*. Tech. rep. ATL-DAQ-2004-011. CERN-ATL-DAQ-2004-011. Geneva: CERN, Sept. 2004. URL: http://cds.cern.ch/record/792528 (cit. on p. 6).

[10] M Shochet et al. *Fast TracKer (FTK) Technical Design Report*. Tech. rep. CERN-LHCC-2013-007. ATLAS-TDR-021. ATLAS Fast Tracker Technical Design Report. June 2013. URL: http://cds.cern.ch/record/1552953 (cit. on p. 8).

[11] ATLAS Collaboration. "Luminosity determination in pp collisions at $\sqrt{s} = 8$ TeV using the ATLAS detector at the LHC". In: *Eur. Phys. J. C* 76 (2016), p. 653. DOI: 10.1140/epjc/s10052-016-4466-1. arXiv: 1608.03953 [hep-ex] (cit. on p. 10).

[12] J. Alwall et al. "The automated computation of tree-level and next-to-leading order differential cross sections, and their matching to parton shower simulations". In: *JHEP* 07 (2014), p. 079. DOI: 10.1007/JHEP07(2014)079. arXiv: 1405.0301 [hep-ph] (cit. on p. 11).

[13] Richard D. Ball et al. "Parton distributions with LHC data". In: *Nucl. Phys. B* 867 (2013), pp. 244–289. DOI: 10.1016/j.nuclphysb.2012.10.003. arXiv: 1207.1303 [hep-ph] (cit. on p. 11).

[14] Torbjorn Sjöstrand, Stephen Mrenna, and Peter Z. Skands. "A Brief Introduction to PYTHIA 8.1". In: *Comput. Phys. Commun.* 178 (2008), p. 852. DOI: 10.1016/j.cpc.2008.01.036. arXiv: 0710.3820 [hep-ph] (cit. on p. 11).

[15] Simone Alioli et al. "A general framework for implementing NLO calculations in shower Monte Carlo programs: the POWHEG BOX". In: *JHEP* 06 (2010), p. 043. DOI: 10.1007/JHEP06(2010)043. arXiv: 1002.2581 [hep-ph] (cit. on p. 11).

[16] Hung-Liang Lai et al. "New parton distributions for collider physics". In: *Phys. Rev. D* 82 (2010), p. 074024. DOI: 10.1103/PhysRevD.82.074024. arXiv: 1007.2241 [hep-ph] (cit. on p. 11).

[17] Pierre Artoisenet et al. "Automatic spin-entangled decays of heavy resonances in Monte Carlo simulations". In: *JHEP* 03 (2013), p. 015. DOI: 10.1007/JHEP03(2013)015. arXiv: 1212.3460 [hep-ph] (cit. on p. 11).

[18] Torbjorn Sjöstrand, Stephen Mrenna, and Peter Z. Skands. "PYTHIA 6.4 Physics and Manual". In: *JHEP* 05 (2006), p. 026. DOI: 10.1088/1126-6708/2006/05/026. arXiv: hep-ph/0603175 (cit. on p. 11).

[19] J. Pumplin et al. "New generation of parton distributions with uncertainties from global QCD analysis". In: *JHEP* 07 (2002), p. 012. DOI: 10.1088/1126-6708/2002/07/012. arXiv: hep-ph/0201195 (cit. on p. 11).

[20] M. Bahr et al. "Herwig++ Physics and Manual". In: *Eur. Phys. J. C* 58 (2008), p. 639. DOI: 10.1140/epjc/s10052-008-0798-9. arXiv: 0803.0883 [hep-ph] (cit. on p. 12).

[21] ATLAS Collaboration. *Modelling of the $t\bar{t}H$ and $t\bar{t}V(V = W, Z)$ processes for $\sqrt{s} =$ 13 TeV ATLAS analyses*. ATL-PHYS-PUB-2016-005. 2016. URL: https://cds.cern.ch/record/2120826 (cit. on p. 12).

[22] T. Gleisberg et al. "Event generation with SHERPA 1.1". In: *JHEP* 02 (2009), p. 007. DOI: 10.1088/1126-6708/2009/02/007. arXiv: 0811.4622 [hep-ph] (cit. on p. 12).

[23] Tanju Gleisberg and Stefan Höche. "Comix, a new matrix element generator". In: *JHEP* 12 (2008), p. 039. DOI: 10.1088/1126-6708/2008/12/039. arXiv: 0808.3674 [hep-ph] (cit. on p. 12).

[24] Fabio Cascioli, Philipp Maierhofer, and Stefano Pozzorini. "Scattering Amplitudes with Open Loops". In: *Phys. Rev. Lett.* 108 (2012), p. 111601. DOI: 10.1103/PhysRevLett.108.111601. arXiv: 1111.5206 [hep-ph] (cit. on p. 12).

[25] Steffen Schumann and Frank Krauss. "A Parton shower algorithm based on Catani-Seymour dipole factorisation". In: *JHEP* 03 (2008), p. 038. DOI: 10.1088/1126-6708/2008/03/038. arXiv: 0709.1027 [hep-ph] (cit. on p. 12).

[26] Stefan Höche et al. "QCD matrix elements + parton showers: The NLO case". In: *JHEP* 04 (2013), p. 027. DOI: 10.1007/JHEP04(2013)027. arXiv: 1207.5030 [hep-ph] (cit. on p. 12).

[27] C. Patrignani et al. (Particle Data Group). "Review of Particle Physics". In: *Chin. Phys. C* 40.10 (2016), p. 100001. DOI: 10.1088/1674-1137/40/10/100001 (cit. on p. 12).

[28] ATLAS Collaboration. *Multi-boson simulation for* 13 *TeV ATLAS analyses*. ATL-PHYS-PUB-2016-002. 2016. URL: https://cds.cern.ch/record/2119986 (cit. on pp. 12, 14).

[29] Richard D. Ball et al. "Parton distributions for the LHC Run II". In: *JHEP* 04 (2015), p. 040. DOI: 10.1007/JHEP04(2015)040. arXiv: 1410.8849 [hep-ph] (cit. on p. 12).

[30] S. Agostinelli et al. "GEANT4: A simulation toolkit". In: *Nucl. Instrum. Meth. A* 506 (2003), pp. 250–303. DOI: 10.1016/S0168-9002(03)01368-8 (cit. on p. 12).

[31] D. J. Lange. "The EvtGen particle decay simulation package". In: *Nucl. Instrum. Meth. A* 462 (2001), p. 152. DOI: 10.1016/S0168-9002(01)00089-4 (cit. on p. 13).

[32] Peter Zeiler Skands. "Tuning Monte Carlo Generators: The Perugia Tunes". In: *Phys. Rev. D* 82 (2010), p. 074018. DOI: 10.1103/PhysRevD.82.074018. arXiv: 1005.3457 [hep-ph] (cit. on p. 13).

[33] ATLAS Collaboration. *ATLAS Pythia 8 tunes to* 7 *TeV data*. ATL-PHYS-PUB-2014-021. 2014. URL: https://cds.cern.ch/record/1966419 (cit. on p. 13).

[34] Stefan Gieseke, Christian Rohr, and Andrzej Siodmok. "Colour reconnections in Herwig++". In: *Eur. Phys. J. C* 72 (2012), p. 2225. DOI: 10.1140/epjc/s10052-012-2225-5. arXiv: 1206.0041 [hep-ph] (cit. on p. 13).

[35] ATLAS Collaboration. *Summary of ATLAS Pythia 8 tunes*. ATL-PHYS-PUB-2012-003. 2012. URL: https://cds.cern.ch/record/1474107 (cit. on p. 13).

[36] A. D. Martin et al. "Parton distributions for the LHC". In: *Eur. Phys. J. C* 63 (2009), p. 189. DOI: 10.1140/epjc/s10052-009-1072-5. arXiv: 0901.0002 [hep-ph] (cit. on p. 13).

[37] W. Beenakker et al. "Squark and gluino production at hadron colliders". In: *Nucl. Phys. B* 492 (1997), pp. 51–103. DOI: 10.1016/S0550-3213(97)00084-9. arXiv: hep-ph/9610490 (cit. on pp. 13, 14).

[38] A. Kulesza and L. Motyka. "Threshold resummation for squark-antisquark and gluino-pair production at the LHC". In: *Phys. Rev. Lett.* 102 (2009), p. 111802. DOI: 10.1103/PhysRevLett.102.111802. arXiv: 0807.2405 [hep-ph] (cit. on pp. 13, 14).

[39] A. Kulesza and L. Motyka. "Soft gluon resummation for the production of gluino-gluino and squark-antisquark pairs at the LHC". In: *Phys. Rev. D* 80 (2009), p. 095004. DOI: 10.1103/PhysRevD.80.095004. arXiv: 0905.4749 [hep-ph] (cit. on pp. 13, 14).

[40] Wim Beenakker et al. "Soft-gluon resummation for squark and gluino hadroproduction". In: *JHEP* 12 (2009), p. 041. DOI: 10.1088/1126-6708/2009/12/041. arXiv: 0909.4418 [hep-ph] (cit. on pp. 13, 14).

[41] W. Beenakker et al. "Squark and gluino hadroproduction". In: *Int. J. Mod. Phys. A* 26 (2011), pp. 2637–2664. DOI: 10.1142/S0217751X11053560. arXiv: 1105.1110 [hep-ph] (cit. on pp. 13, 14).

[42] Christoph Borschensky et al. "Squark and gluino production cross sections in pp collisions at $\sqrt{s} = 13$, 14, 33 and 100 TeV". In: *Eur. Phys. J.* C74.12 (2014), p. 3174. DOI: 10.1140/epjc/s10052-014-3174-y. arXiv: 1407.5066 [hep-ph] (cit. on pp. 13, 14).

[43] ATLAS Collaboration. "Search for squarks and gluinos with the ATLAS detector in final states with jets and missing transverse momentum using 4.7 fb^{-1} of $\sqrt{s} = 7$ TeV proton-proton collision data". In: *Phys. Rev. D* 87.1 (2013), p. 012008. DOI: 10.1103/PhysRevD.87.012008. arXiv: 1208.0949 [hep-ex] (cit. on p. 13).

[44] Michal Czakon and Alexander Mitov. "Top++: A Program for the Calculation of the Top-Pair Cross-Section at Hadron Colliders". In: *Comput. Phys. Commun.* 185 (2014), p. 2930. DOI: 10.1016/j.cpc.2014.06.021. arXiv: 1112.5675 [hep-ph] (cit. on p. 14).

[45] Nikolaos Kidonakis. "Next-to-next-to-leading-order collinear and soft gluon corrections for t-channel single top quark production". In: *Phys. Rev. D* 83 (2011), p. 091503. DOI: 10.1103/PhysRevD.83.091503. arXiv: 1103.2792 [hep-ph] (cit. on p. 14).

[46] Nikolaos Kidonakis. "Two-loop soft anomalous dimensions for single top quark associated production with a W^- or H^-". In: *Phys. Rev. D* 82 (2010), p. 054018. DOI: 10.1103/PhysRevD.82.054018. arXiv: 1005.4451 [hep-ph] (cit. on p. 14).

[47] Nikolaos Kidonakis. "NNLL resummation for s-channel single top quark production". In: *Phys. Rev. D* 81 (2010), p. 054028. DOI: 10.1103/PhysRevD.81.054028. arXiv: 1001.5034 [hep-ph] (cit. on p. 14).

[48] D. de Florian et al. "Handbook of LHC Higgs Cross Sections: 4. Deciphering the Nature of the Higgs Sector". In: (2016). DOI: 10.23731/CYRM-2017-002. arXiv: 1610.07922 [hep-ph] (cit. on p. 14).

[49] J R Andersen et al. "Handbook of LHC Higgs Cross Sections: 3. Higgs Properties". In: (2013). DOI: 10.5170/CERN-2013-004. arXiv: 1307.1347 [hep-ph] (cit. on p. 14).

[50] Stefano Catani et al. "Vector boson production at hadron colliders: a fully exclusive QCD calculation at NNLO". In: *Phys. Rev. Lett.* 103 (2009), p. 082001. DOI: 10.1103/PhysRevLett.103.082001. arXiv: 0903.2120 [hep-ph] (cit. on p. 14).

[51] M (CERN) Aleksa et al. *ATLAS Liquid Argon Calorimeter Phase-I Upgrade Technical Design Report*. Tech. rep. CERN-LHCC-2013-017. ATLAS-TDR-022. Final version presented to December 2013 LHCC. Sept. 2013. URL: https://cds.cern.ch/record/1602230 (cit. on p. 15).

[52] *Letter of Intent for the Phase-I Upgrade of the ATLAS Experiment*. Tech. rep. CERN-LHCC-2011-012. LHCC-I-020. Geneva: CERN, Nov. 2011. URL: https://cds.cern.ch/record/1402470 (cit. on p. 15).

[53] Michael Begel et al. *Global Feature Extractor of the Level-1 Calorimeter Trigger: ATLAS TDAQ Phase-I Upgrade gFEX Final Design Report*. Tech. rep. ATL-COM-DAQ-2016-184. Geneva: CERN, Nov. 2016. URL: https://cds.cern.ch/record/2233958 (cit. on pp. 15–17, 19, 20).

[54] John Thomas Anderson et al. *FELIX: a High-Throughput Network Approach for Interfacing to Front End Electronics for ATLAS Upgrades*. Tech. rep. ATL-DAQ-PROC-2015-014. 8. Geneva: CERN, May 2015. URL: https://cds.cern.ch/record/2016626 (cit. on p. 16).